Physics of Massive Neutrinos

J. W. F. Valle[a*]

[a]AHEP Group, Instituto de Física Corpuscular – C.S.I.C./Universitat de València
Edificio Institutos de Paterna, Apt 22085, E–46071 Valencia, Spain

I summarize the present status of global analyses of neutrino oscillations, including the most recent KamLAND and K2K data, as well as the latest solar and atmospheric neutrino fluxes. I give the allowed ranges of the three–flavour oscillation parameters from the current worlds' global neutrino data sample, their best fit values and discuss the small parameters $\alpha \equiv \Delta m^2_{\rm SOL}/\Delta m^2_{\rm ATM}$ and $\sin^2\theta_{13}$, which characterize the strength of CP violation in neutrino oscillations. I briefly discuss neutrinoless double beta decay and the LSND neutrino oscillation hint, as well as the robustness of the neutrino oscillation results in the presence of non-standard physics.

1. INTRODUCTION

The discovery of neutrino oscillations by combining data from solar [1], atmospheric [2], reactor [3] and accelerator [4] neutrino studies has marked a turning point in our understanding of nature and has brought neutrino physics to the center of attention of the particle, nuclear and astrophysics communities. This culminates a heroic effort which started over four decades ago and now firmly establishes the existence of small neutrino masses, confirming theoretical expectations which date back to the early eighties. Neutrino mass arise from the dimension-five operator $\ell\ell\phi\phi$ where ϕ the $SU(2)\otimes U(1)$ Higgs doublet and ℓ is a lepton doublet [5]. Nothing is known from first principles about the mechanism that induces this operator, its associated mass scale or flavour structure. Its most popular realization is the seesaw mechanism which induces small neutrino masses from the exchange of heavy states. Although inspired by unification, the effective model-independent description of the seesaw at low-energies is in terms of the $SU(2)\otimes U(1)$ gauge structure and contains a small effective Higgs triplet contribution to the neutrino mass [6]. Such general seesaw has 24 parameters, 3 more than the tripletless case [6] [2].

The structure of the three-flavour lepton mixing matrix in various gauge theories of neutrino mass was given in [6] and it was also argued that, on *general* grounds, massive neutrinos should be Majorana particles, leading to neutrinoless double beta decay ($\beta\beta_{0\nu}$) [8]. Current neutrino oscillation data are well described by the simplest unitary lepton mixing matrix neglecting CP violation. The effect of Dirac CP phases in oscillations and Majorana phases in $\beta\beta_{0\nu}$ constitute the main challenge for the years to come.

Here I focus mainly on the determination of neutrino mass and mixing parameters in neutrino oscillation studies, a currently thriving industry [9], with many new experiments currently underway or planned. The interpretation of the data requires good calculations of solar and atmospheric neutrino fluxes [10,11], neutrino cross sections and experimental response functions, as well as a careful description of neutrino propagation both in the Sun and the Earth, including matter effects [12,13]. After summarizing the latest (post-Neutrino-2004) global analysis of 3-

*Work supported by grant BFM2002-00345, by EC RTN grant HPRN-CT-2000-00148 and ESF *Neutrino Astrophysics Network*. Latest neutrino oscillation plots are taken from a review with Maltoni, Schwetz and Tortola.

[2]In the mass basis these correspond to the 12 mixing angles and 12 CP phases (both Dirac and Majorana-type) that characterize the full 3×6 charged current seesaw lepton mixing matrix [6]. These are exactly the same parameters involved in the description of leptogenesis [7], though in this case the use of the weak basis seems more convenient. Note also that current nomenclature (type-I versus II seesaw) is opposite from the original one in [6].

neutrino oscillation parameters [14] [15] I briefly discuss their impact on future $\beta\beta_{0\nu}$ searches [16]. This writeup combines my plenary talk and the WG1 parallel session talk on non-standard scenarios of neutrino conversion.

2. TWO-NEUTRINO OSCILLATIONS

Let us first consider neutrino oscillations in the two-flavour approximation [14].

2.1. Solar + KamLAND

The solar neutrino data includes the measured rates of the chlorine experiment at the Homestake mine ($2.56 \pm 0.16 \pm 0.16$ SNU), the most up-to-date results of the gallium experiments SAGE ($66.9\ ^{+3.9}_{-3.8}\ ^{+3.6}_{-3.2}$ SNU) and GALLEX/GNO ($69.3 \pm 4.1 \pm 3.6$ SNU), as well as the 1496–day Super-K data in the form of 44 bins (8 energy bins, 6 of which are further divided into 7 zenith angle bins). The SNO data include the most recent data from the salt phase in the form of the neutral current (NC), charged current (CC) and elastic scattering (ES) fluxes, as well as the 2002 spectral day/night data (17 energy bins for each day and night period).

The analysis methods are described in [19] and references therein [15]. We use a generalization of the pull approach for the χ^2 calculation originally suggested in Ref. [20] in which all systematic uncertainties such as those of the eight solar neutrino fluxes are included by introducing new parameters in the fit and adding a penalty function to the χ^2. The method [14,19] is exact to all orders in the pulls and covers the case of correlated statistical errors [21] as necessary to treat the SNO–salt experiment. This is particularly interesting as it allows us to include the Standard Solar Model ^{8}B flux prediction as well as the SNO NC measurement on the same footing, without pre-selecting a particular value, as implied by expanding around the predicted value: the fit itself chooses the best compromise between the SNO NC data and the SSM prediction.

KamLAND detects reactor anti-neutrinos at the Kamiokande site by the process $\bar{\nu}_e + p \to e^+ + n$, where the delayed coincidence of the prompt energy from the positron and a characteristic gamma from the neutron capture allows an efficient reduction of backgrounds. Most of the incident $\bar{\nu}_e$ flux comes from nuclear plants at distances of $80 - 350$ km from the detector, far enough to probe the LMA solution of the solar neutrino problem. The neutrino energy is related to the prompt energy by $E_\nu = E_{\rm pr} + \Delta - m_e$, where Δ is the neutron-proton mass difference and m_e is the positron mass. For lower energies there is a relevant contribution from geo-neutrino events to the signal [22]. To avoid large uncertainties associated with the geo-neutrino flux an energy cut at 2.6 MeV prompt energy is applied for the oscillation analysis.

First KamLAND results were taken from March to October 2002. Data corresponding to a 162 ton-year exposure gave 54 anti-neutrino events in the final sample, after all cuts, while 86.8 ± 5.6 events are predicted for no oscillations with 0.95 ± 0.99 background events. The probability that the KamLAND result is consistent with the no–disappearance hypothesis is less than 0.05%. This gave the first evidence for the disappearance of neutrinos traveling to a detector from a power reactor and the first terrestrial confirmation of the solar neutrino anomaly.

New KamLAND data were presented at Neutrino 2004 [3]. With a somewhat larger fiducial volume of the detector an exposure corresponding to 766.3 ton-year has been obtained between March 2002 and January 2004 (including a reanalysis of the previous 2002 data). In total 258 events have been observed, versus 356.2 ± 23.7 reactor neutrino events expected in the case of no disappearance and 7.5 ± 1.3 background events. This leads to a confidence level of 99.995% for $\bar{\nu}_e$ disappearance, and the averaged survival probability is $0.686 \pm 0.044({\rm stat}) \pm 0.045({\rm syst})$. Moreover evidence for spectral distortion consistent with oscillations is obtained [3].

It is convenient to treat the latest KamLAND data binning them equally in $1/E_{\rm pr}$, instead of the traditional bins of equal size in $E_{\rm pr}$. Various systematic errors associated to the neutrino fluxes, backgrounds, reactor fuel composition and individual reactor powers, small matter effects, and improved $\bar{\nu}_e$ flux parameterization are included [14]. One finds a beautiful agreement be-

tween KamLAND data and the region implied by the LMA solution to the solar neutrino problem, which in this way has been singled out as the only viable one in contrast to the previous "zoo" of oscillation solutions [19,23]. However the stronger evidence for spectral distortion in the recent data leads to improved information on $\Delta m^2_{\rm SOL}$, substantially reducing the allowed region of oscillation parameters. From this point of view KamLAND has played a fundamental role in the resolution of the solar neutrino problem.

Assuming CPT invariance one can directly compare the information obtained from solar neutrino experiments with the KamLAND reactor results. In Fig. 1 we show the allowed regions from the combined analysis of solar and KamLAND data.

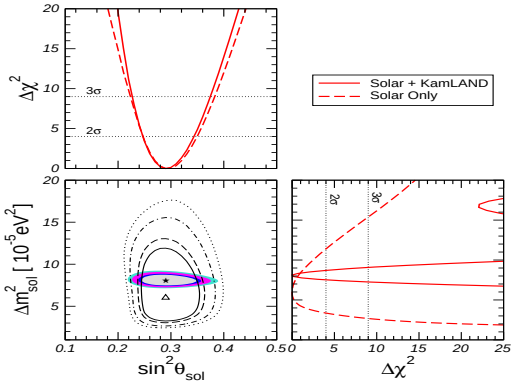

Figure 1. Regions allowed by solar+KamLAND data at 90%, 95%, 99%, and 3σ C.L. for 2 d.o.f.. Unshaded regions correspond to solar data only.

2.2. Atmospheric + K2K

The zenith angle dependence of the μ-like atmospheric neutrino data from the Super-K experiment provided the first evidence for neutrino oscillations in 1998, an effect confirmed also by other atmospheric neutrino experiments [2]. The dip in the L/E distribution of the atmospheric ν_μ survival probability seen in Super-K gives a clearer signature for neutrino oscillations.

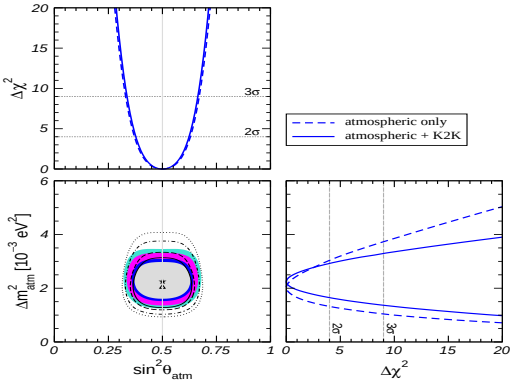

Figure 2. $\sin^2\theta_{\rm ATM}$–$\Delta m^2_{\rm ATM}$ regions allowed at 90%, 95%, 99%, and 3σ C.L. for 2 d.o.f. (the unshaded regions include atmospheric data only).

The analysis summarized below includes the most recent charged-current atmospheric neutrino data from Super-K, with the e-like and μ-like data samples of sub- and multi-GeV contained events grouped into 10 zenith-angle bins, with 5 angular bins of stopping muons and 10 through-going bins of up-going muon events. No information on ν_τ appearance, multi-ring μ and neutral-current events is used since an efficient Monte-Carlo simulation of these data would require more details of the Super-K experiment, in particular of the way the neutral-current signal is extracted from the data (see Refs. [19,23] for details). Here the new three–dimensional atmospheric neutrino fluxes given in [11] are used, in contrast to previous analyses using the Bartol fluxes [24]. With this one obtains the regions of two-flavour $\nu_\mu \to \nu_\tau$ oscillation parameters $\sin^2\theta_{\rm ATM}$ and $\Delta m^2_{\rm ATM}$ shown by the hollow contours in Fig. 2. One notes that the $\Delta m^2_{\rm ATM}$ values obtained with the three–dimensional atmospheric neutrino fluxes are lower than obtained previously [19], in excellent agreement with the results of the Super-K collaboration [25].

The KEK to Kamioka (K2K) long-baseline neutrino oscillation experiment [4] probes ν_μ dis-

appearance in the same Δm^2 region as probed with atmospheric neutrinos. The neutrino beam is produced by a 12 GeV proton beam from the KEK proton synchrotron, and consists of 98% muon neutrinos with a mean energy of 1.3 GeV. The beam is controlled by a near detector 300 m away from the proton target. Information on neutrino oscillations is obtained by the comparing this near detector data with the ν_μ content of the beam observed by the Super-Kamiokande detector at a distance of 250 km.

The data K2K-I sample has been collected in the period from June 1999 to July 2001 (4.8×10^{19} protons on target) and gave 56 events in Super-K, whereas $80.1^{+6.2}_{-5.4}$ were expected for no oscillations. The probability that the observed flux is explained by a statistical fluctuation without neutrino oscillations is less than 1% [4]. K2K-II started in Fall 2002, and released data at the Neutrino2004 conference [4] corresponding to 4.1×10^{19} protons on target, comparable to the K2K-I sample. Altogether K2K-I and K2K-II give 108 events in Super-K, to be compared with $150.9^{+11.6}_{-10.0}$ expected for no oscillations. Out of the 108 events 56 are so-called single-ring muon events. This data sample contains mainly muon events from the quasi-elastic scattering $\nu_\mu + p \to \mu + n$, and the reconstructed energy is closely related to the true neutrino energy. The K2K collaboration finds that the observed spectrum is consistent with the one expected for no oscillation only at a probability of 0.11%, whereas the spectrum predicted by the best fit oscillation parameters has a probability of 52% [4].

The re-analysis of K2K data given in [14] uses the energy spectrum of the 56 single-ring muon events from K2K-I + K2K-II (unfortunately not the full K2K data sample of 108 events, for lack of information outside the K2K collaboration). Under reasonable assumptions, one can fit the data divided into 15 bins in reconstructed neutrino energy. One finds that the neutrino mass-squared difference indicated by the ν_μ disappearance in K2K agrees with atmospheric neutrino results, providing the first confirmation of oscillations with $\Delta m^2_{\rm ATM}$ from a man-made neutrino source. However K2K gives a rather weak constraint on the mixing angle due to low statistics in the current data sample.

The shaded regions in Fig. 2 are the allowed ($\sin^2\theta_{\rm ATM}$, $\Delta m^2_{\rm ATM}$) regions that follow from the combined analysis of K2K and Super-K atmospheric neutrino data. One sees that, although the determination of $\sin^2\theta_{\rm ATM}$ is completely dominated by atmospheric data, the K2K data start already to constrain the allowed region of $\Delta m^2_{\rm ATM}$. Note also that, despite the downward shift of $\Delta m^2_{\rm ATM}$ implied by the new atmospheric fluxes, the new result is statistically compatible both with the previous one in [19] and with the value obtained by the Super-K L/E analysis [2]. Note that the K2K constraint on $\Delta m^2_{\rm ATM}$ from below is important for future long-baseline experiments, as such experiments are drastically affected if $\Delta m^2_{\rm ATM}$ lies in the lower part of the 3σ range indicated by the atmospheric data alone.

3. THREE-NEUTRINO OSCILLATIONS

The effective leptonic mixing matrix in gauge theories of massive neutrinos was systematically studied in [6]. For high-scale seesaw models this matrix is approximately unitary and, for three neutrinos, may be taken as [26] [3]

$$K = \omega_{23}\omega_{13}\omega_{12} \tag{1}$$

where each factor, for example,

$$\omega_{13} = \begin{pmatrix} c_{13} & 0 & e^{i\phi_{13}}s_{13} \\ 0 & 1 & 0 \\ -e^{-i\phi_{13}}s_{13} & 0 & c_{13} \end{pmatrix}.$$

contains an angle and a CP phase. Two of the three angles are involved in solar and atmospheric oscillations, so we set $\theta_{12} \equiv \theta_{\rm SOL}$ and $\theta_{23} \equiv \theta_{\rm ATM}$. All these three phases are physical [32], one corresponds to the one present in the quark sector (Dirac-phase) and affects neutrino oscillations, while the other two are associated to the Majorana nature of neutrinos and show up in neutrinoless double beta decay and other lepton-number violating processes, but not in conventional neutrino oscillations [32,33].

[3] This also holds in radiative models [27,28] and models where supersymmetry is the origin of neutrino mass [29]. In inverse seesaw models [30] deviations from unitarity may be phenomenologically important [31].

parameter	best fit	3σ range
Δm^2_{21} [10^{-5} eV^2]	8.1	7.2–9.1
Δm^2_{31} [10^{-3} eV^2]	2.2	1.4–3.3
$\sin^2\theta_{12}$	0.30	0.23–0.38
$\sin^2\theta_{23}$	0.50	0.34–0.68
$\sin^2\theta_{13}$	0.000	≤ 0.047

Table 1
Three–neutrino oscillation parameters from the global data analysis given in [14].

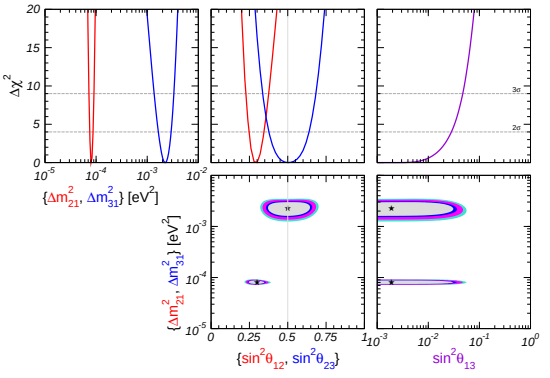

Figure 3. Three–neutrino regions allowed by the world's oscillation data at 90%, 95%, 99%, and 3σ C.L. for 2 d.o.f. Top panels give $\Delta\chi^2$ minimized with respect to all undisplayed parameters.

Current neutrino oscillation experiments are insensitive to CP violation, thus all phases will be neglected (future neutrino factories aim at probing the effects of the Dirac phase [34]). In this approximation three-neutrino oscillations depend on the three mixing parameters $\sin^2\theta_{12}, \sin^2\theta_{23}, \sin^2\theta_{13}$ and on the two mass-squared differences $\Delta m^2_{\rm SOL} \equiv \Delta m^2_{21} \equiv m^2_2 - m^2_1$ and $\Delta m^2_{\rm ATM} \equiv \Delta m^2_{31} \equiv m^2_3 - m^2_1$ characterizing solar and atmospheric neutrinos. The hierarchy $\Delta m^2_{\rm SOL} \ll \Delta m^2_{\rm ATM}$ implies that one can set, to a good approximation, $\Delta m^2_{\rm SOL} = 0$ in the analysis of atmospheric and K2K data, and $\Delta m^2_{\rm ATM}$ to infinity in the analysis of solar and KamLAND data. The relevant neutrino oscillation data in a global three-neutrino analysis are those of sections 2.1 and 2.2 together with the constraints from the CHOOZ and Palo Verde reactor experiments [35].

The results of the global three–neutrino analysis are summarized in Fig. 3 and in Tab. 1. In the upper panels of the figure the $\Delta\chi^2$ is shown as a function of the parameters $\sin^2\theta_{12}, \sin^2\theta_{23}, \sin^2\theta_{13}, \Delta m^2_{21}, \Delta m^2_{31}$, minimized with respect to the undisplayed parameters. The lower panels show two-dimensional projections of the allowed regions in the five-dimensional parameter space. The best fit values and the allowed 3σ ranges of the oscillation parameters from the global data are summarized in Tab. 1. This table gives the current status of the three–flavour neutrino oscillation parameters.

In a three–neutrino scheme CP violation disappears when two neutrinos become degenerate [6] or when one angle vanihes, $\theta_{13} \to 0$ [36]. Genuine three–flavour effects are associated to the mass hierarchy parameter $\alpha \equiv \Delta m^2_{\rm SOL}/\Delta m^2_{\rm ATM}$ and the mixing angle θ_{13}. The left panel in Fig. 4 gives the parameter α as determined from the global χ^2 analysis of [14]. The figure also gives $\Delta\chi^2$ as a function of the parameter combination $\alpha \sin 2\theta_{12}$ which, to leading order, determines the long baseline $\nu_e \to \nu_\mu$ oscillation probability [37,38]. The last unknown angle in the three–neutrino leptonic mixing matrix is θ_{13}, for which only an upper bound exists. The leftt panel in Fig. 4 gives $\Delta\chi^2$ as a function of $\sin^2\theta_{13}$ for different data sample choices. One finds that the new data from KamLAND have a surprisingly strong impact on this bound. Before the KamLAND-2004 data the bound on $\sin^2\theta_{13}$ from global data was dominated by the CHOOZ reactor experiment, together with the determination of Δm^2_{31} from atmospheric data. However, with the KamLAND-2004 data the bound becomes comparable to the reactor bound, and contribute significantly to the final global bound 0.022 (0.047) at 90% C.L. (3σ) for 1 d.o.f. This improved $\sin^2\theta_{13}$ bound follows from the strong spectral distortion found in the 2004 sample [14]. Note that, since the CHOOZ bound on $\sin^2\theta_{13}$ deteriorates quickly as $\Delta m^2_{\rm ATM}$ decreases (see Fig. 5), the improvement is espe-

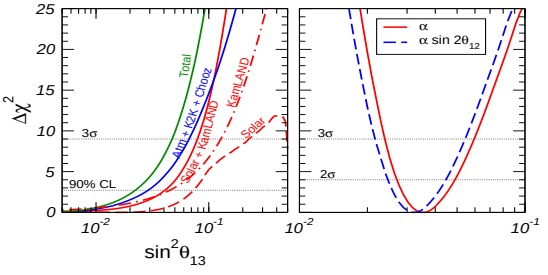

Figure 4. Determination of $\alpha \equiv \Delta m^2_{\rm SOL}/\Delta m^2_{\rm ATM}$ and bound on $\sin^2\theta_{13}$ from current neutrino oscillation data.

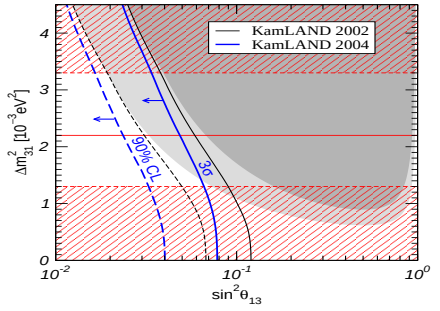

Figure 5. Upper bound on $\sin^2\theta_{13}$ (1 d.o.f.) from solar+KamLAND+CHOOZ data versus $\Delta m^2_{\rm ATM}$. Dashed (solid) curves correspond to 90% (3σ) C.L. bounds, thick curves include KamLAND-2004 data, thin ones do not. Light (dark) regions are excluded by CHOOZ at 90% (3σ) C.L. The horizontal line corresponds to the current $\Delta m^2_{\rm ATM}$ best fit value, hatched regions are excluded by atmospheric + K2K data at 3σ.

cially important for lower $\Delta m^2_{\rm ATM}$ values, as implied by the new three–dimensional atmospheric fluxes [11]. In Fig. 5 we show the upper bound on $\sin^2\theta_{13}$ as a function of $\Delta m^2_{\rm ATM}$ from CHOOZ data alone compared to the bound from an analysis including solar and reactor neutrino data. One finds that, although for larger $\Delta m^2_{\rm ATM}$ values the bound on $\sin^2\theta_{13}$ is dominated by CHOOZ, for $\Delta m^2_{\rm ATM} \lesssim 2\times 10^{-3}{\rm eV}^2$ the solar + KamLAND data start being relevant. The bounds implied by the 2002 and 2004 KamLAND data are compared in Fig. 5. In addition to reactor and accelerator neutrino oscillation searches (Lindners' talk), future studies of the day/night effect in large water Cerenkov solar neutrino experiments like UNO or Hyper-K [39] may improve the sensitivity on $\sin^2\theta_{13}$ [40].

4. ABSOLUTE NEUTRINO MASSES

Neutrino oscillation data are sensitive only to mass differences, not to the absolute neutrino masses. Nor do they have any bearing on the fundamental issue of whether neutrinos are Dirac or Majorana particles [32,33]. The significance of the $\beta\beta_{0\nu}$ decay is given by the fact that, in a gauge theory, irrespective of the mechanism that induces $\beta\beta_{0\nu}$, it is bound to also yield a Majorana neutrino mass [41], as illustrated in Fig. 6. Quantitative implications of the "black-box" argument are model-dependent, but the theorem holds in any "natural" gauge theory.

Now that oscillations are experimentally confirmed we know that $\beta\beta_{0\nu}$ must be induced by the exchange of light Majorana neutrinos. The corresponding amplitude is sensitive both to the absolute scale of neutrino mass as well as the two Majorana CP phases that characterize the minimal 3-neutrino mixing matrix [6]. Fig. 7 shows the estimated average mass parameter characterizing the neutrino exchange contribution to $\beta\beta_{0\nu}$ versus the lightest neutrino mass. The upper

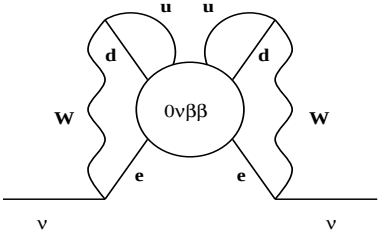

Figure 6. Equivalence between $\beta\beta_{0\nu}$ and Majorana mass in gauge theories [41].

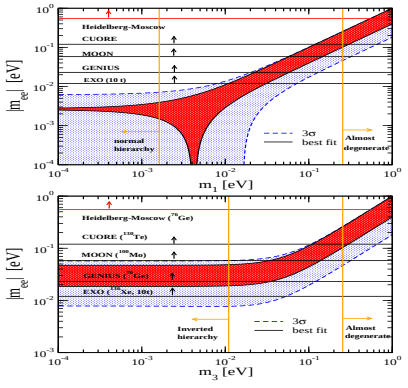

Figure 7. Neutrino-mass-induced $\beta\beta_{0\nu}$ from current oscillation data versus current and projected experimental sensitivities.

(lower) panel corresponds to the cases of normal (inverted) neutrino mass spectra. The calculation takes into account the current neutrino oscillation parameters from [14] and the nuclear matriz elements of [16]. In contrast to the normal hierarchy, where a destructive interference of neutrino amplitudes is possible, the inverted neutrino mass hierarchy implies a "lower" bound for the $\beta\beta_{0\nu}$ amplitude. Quasi-degenerate neutrinos [42,43] such as predicted in [17], give the largest $\beta\beta_{0\nu}$ amplitude. Future experiments [44] will provide an independent confirmation of the Heidelberg-Moscow results [45] and extend the sensitivity to inverse hierarchy models.

Complementary information on the absolute scale of neutrino mass comes from beta decays searches [46] as well as cosmology [47].

5. FOUR-NEUTRINO OSCILLATIONS?

In addition to the strong evidence for oscillations of solar and atmospheric neutrinos there is also a hint for oscillations from LSND [48]. This accelerator experiment at Los Alamos observed $87.9 \pm 22.4 \pm 6.0$ excess events in the $\bar{\nu}_\mu \to \bar{\nu}_e$ appearance channel, corresponding to a transition probability of $P = (0.264 \pm 0.067 \pm 0.045)\%$, which is $\sim 3.3\ \sigma$ away from zero. To explain this signal with neutrino oscillations requires a mass-squared difference $\Delta m^2_{\rm LSND} \sim 1$ eV^2, a value inconsistent with the solar+KamLAND and atmospheric+K2K experiments described above. Four–neutrino schemes [42,49,50] where a sterile neutrino is added to the three active ones might provide the additional mass scale needed to reconcile the LSND evidence.

The updated analysis described in [14] includes, in addition to LSND, solar+KamLAND and atmospheric+K2K data, also the data from short-baseline (SBL) accelerator and reactor experiments with no evidence for oscillations. The oscillation data are divided into the four sets $X =$ SOL, ATM, NEV, LSND and the PG method is used to test their statistical compatibility in a given mass scheme. Following Ref. [51] we consider the contributions to $\Delta\chi^2_X = \chi^2_X - (\chi^2_X)_{\rm min}$ from different data samples (see [52] for more details). In Tab. 2 we show the contributions of the 4 data sets to $\chi^2_{\rm PG} \equiv \bar{\chi}^2_{\rm min}$ for (3+1) and (2+2) oscillation schemes. As expected we note that in (3+1) schemes the main contribution comes from SBL data due to the tension between LSND and NEV data in these schemes. For (2+2) schemes a large part of $\chi^2_{\rm PG}$ comes from solar and atmospheric data, due to the rejection against a sterile neutrino contribution of these two data sets. The contribution from NEV data in (2+2) comes mainly from the tension between LSND and KARMEN [53], which does not depend on the mass scheme. The parameter goodness of fit is obtained by evaluating $\chi^2_{\rm PG}$ for 4 d.o.f. [54]. Using an improved goodness of fit method especially sensitive to the combination of data sets one finds that (2+2) schemes are ruled out at the 4.9σ level. The inclusion of MACRO data in the analysis would further improve the degree of rejection of these schemes. Note that such a strong rejection of (2+2) schemes holds irrespective of whether LSND is confirmed or not.

Although none of the four–neutrino schemes provides a good fit to the global oscillation data including LSND, it is interesting to consider the *relative* status of the three hypotheses (3+1), (2+2) and the three–active neutrino scenario (3+0). This is done by comparing the χ^2 value of the best fit point – which occurs for the (3+1)

	SOL	ATM	LSND	NEV	$\chi^2_{\rm PG}$	PG
(3+1)	0.0	0.4	5.7	10.9	17.0	1.9×10^{-3} (3.1σ)
(2+2)	5.3	20.8	0.6	7.3	33.9	7.8×10^{-7} (4.9σ)

Table 2
Contributions of different data sets to $\chi^2_{\rm PG}$ in (3+1) and (2+2) neutrino mass schemes.

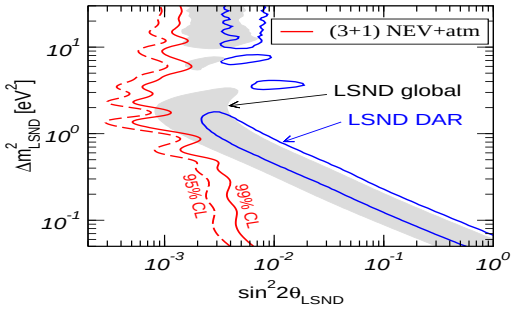

Figure 8. Upper bound on $\sin^2 2\theta_{\rm LSND}$ from NEV, atmospheric and K2K data in (3+1) schemes. The dotted line corresponds to the 99% C.L. bound without K2K and using the 1-d Bartol flux. Also shown are the regions allowed at 99% C.L. (2 d.o.f.) from global LSND data and decay-at-rest (DAR) LSND data.

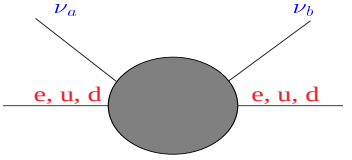

Figure 9. Flavour-changing effective operator.

scheme – with the ones corresponding to (2+2) and (3+0). First we observe that (2+2) schemes are strongly disfavored with respect to (3+1) with a $\Delta\chi^2 = 16.9$. For 4 d.o.f. this is equivalent to an exclusion at 3.1σ. Furthermore, one finds that (3+0) is disfavored with a $\Delta\chi^2 = 17.5$ (corresponding to 3.2σ for 4 d.o.f.) with respect to (3+1), reflecting the high statistical significance of the LSND result.

On the other hand (3+1) spectra are disfavored by the disagreement of LSND with short-baseline disappearance data of CDHS and Bugey, leading to a marginal GOF of 1.9×10^{-3} (3.1σ). Should LSND be confirmed a positive signal is predicted right at the edge of the current sensitivity. In Fig. 8 we give the upper bound on the LSND oscillation amplitude $\sin^2 2\theta_{\rm LSND}$ from the combined analysis of NEV and atmospheric neutrino data. From the figure one sees that the bound is incompatible with the signal observed in LSND at the 95% C.L. Marginal overlap regions between the bound and global LSND data exist only if both are taken at 99% C.L. Restricting to the decay-at-rest LSND data sample [53] makes the disagreement even more severe. This shows that 4-neutrino descriptions of LSND do not provide a satisfactory fit to the world's neutrino data. Although a reasonable 5-neutrino fit is possible, the confirmation of LSND is essential.

6. BEYOND OSCILLATIONS

Non-standard physics may in principle affect neutrino propagation properties and detection cross sections [55]. Such interactions (NSI, for short) are a natural outcome of many neutrino mass models [56] and can be of two types: flavour-changing (FC) and non-universal (NU). They may arise from a nontrivial structure of charged and neutral current weak interactions with non-unitary lepton mixing matrix [6] as expected in inverse seesaw models [30,31], in radiative neutrino mass models [27,28] and in supersymmetric unified models [57]. NSI may be schematically represented as effective dimension-6 terms of the sub-weak strength εG_F, see Fig. 9.

In the presence of NSI, the Hamiltonian describing atmospheric neutrino propagation has, in addition to the standard oscillation part, another term $H_{\rm NSI}$ accounting for an effective potential

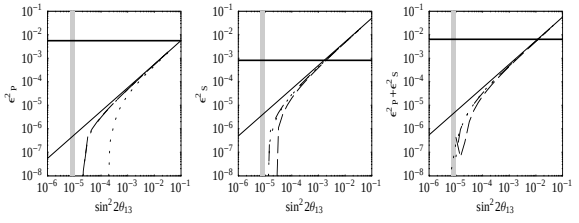

Figure 10. Deterioration of θ_{13} at a neutrino factory in the presence of NSI, explanation in [61]

induced by the NSI with matter:

$$H_{\rm NSI} = \pm\sqrt{2}G_F N_f \begin{pmatrix} 0 & \varepsilon \\ \varepsilon & \varepsilon' \end{pmatrix} . \qquad (2)$$

Here $+(-)$ holds for neutrinos (anti-neutrinos) and ε and ε' parameterize the NSI: $\sqrt{2}G_F N_f \varepsilon$ is the forward scattering amplitude for the FC process $\nu_\mu + f \to \nu_\tau + f$ and $\sqrt{2}G_F N_f \varepsilon'$ represents the difference between $\nu_\mu + f$ and $\nu_\tau + f$ elastic forward scattering. Here N_f is the number density of the fermion f along the neutrino path.

The impact of non-standard neutrino interactions on the determination of atmospheric neutrino parameters $\Delta m^2_{\rm ATM}$ and $\sin^2\theta_{\rm ATM}$ was considered in Ref. [58] treating the NSI strengths as free phenomenological parameters and taking for f the down-type quark, for definiteness. This analysis takes into account both the effect of $\nu_\mu \to \nu_\tau$ oscillations as well as the existence of non-standard neutrino–matter interactions in this channel. It is shown that, in the 2-neutrino approximation, the determination of the atmospheric neutrino oscillation parameters $\Delta m^2_{\rm ATM}$ and $\sin^2 2\theta_{\rm ATM}$ is practically unaffected by the presence of NSI. Future neutrino factories will substantially improve this bound [59]. In contrast, as shown in [60] the determination of solar neutrino parameters is still not yet fully robust against the presence of NSI. Before concluding, let me mention that, even a small residual non-standard interaction of neutrinos in the $e-\tau$ channel leads to a drastic loss in sensitivity in the determination θ_{13} through the so-called "golden channels" at a neutrino factory [61], see Fig. 10. This may only be partly overcome by combining if different baselines. Only by rejecting NSI at a near detector can one improve sensitivities in θ_{13}.

7. CONCLUSION

Experiment is ahead of theory in neutrino physics: despite the great progress achieved recently we are very far from a "road map" to the ultimate theory of neutrino properties. We have no idea of the underlying neutrino mass generation mechanism, its characteristic scale or its flavor structure. We have still a long way to go!

REFERENCES

1. T. Mitsui, these proceedings.
2. T. Kajita, these proceedings.
3. G. Gratta, Neutrino 2004 proceedings.
4. T. Nakaya, Neutrino 2004 proceedings.
5. S. Weinberg, Phys. Rev. **D22** 1694 (1980).
6. J. Schechter and J. W. F. Valle, Phys. Rev. **D22**, 2227 (1980); **D25**, 774 (1982).
7. M. Fukugita and T. Yanagida, Phys. Lett. B **174** (1986) 45.
8. L. Wolfenstein, Phys. Lett. B **107** 77 (1981); J. Schechter and J. W. F. Valle, Phys. Rev. **D24**, 1883 (1981), Err. D25, 283 (1982); see also talks by L. Wolfenstein and J. W. F. Valle at Joe's Fest, AIP Conf. Proc. **687**, 16 (2003)
9. M. Goodman, Neutrino Oscillation Industry Web-Page, http://neutrinooscillation.org/.
10. J. N. Bahcall and M. H. Pinsonneault, Phys. Rev. Lett. **93**, 121301 (2004)
11. M. Honda, T. Kajita, K. Kasahara and S. Midorikawa, astro-ph/0404457.
12. S. P. Mikheev and A. Y. Smirnov, Sov. J. Nucl. Phys. **42**, 913 (1985).
13. L. Wolfenstein, Phys. Rev. **D17**, 2369 (1978).
14. M. Maltoni, T. Schwetz, M. A. Tortola and J. W. F. Valle, New J. Phys. 6 (2004) 122 [hep-ph/0405172] and references therein.
15. S. Goswami, talk at Neutrino 2004.
16. S. M. Bilenky, A. Faessler and F. Simkovic, Phys. Rev. **D70** 033003 (2004)
17. K. Babu, E. Ma and J. W. F. Valle, Phys. Lett. **B552** 207 (2003); M. Hirsch et al, Phys. Rev. D **69** 093006 (2004)

18. C. H. Albright, hep-ph/0407155; W. Grimus et al, hep-ph/0408123; S. M. Barr and I. Dorsner, Nucl. Phys. B **585** 79 (2000); H. S. Goh et al, Phys. Lett. B **587** 105 (2004); M. Raidal, hep-ph/0404046; H. Minakata and A. Y. Smirnov, hep-ph/0405088; G. Altarelli and F. Feruglio, Proc. of 10th Int. Workshop on Neutrino Telescopes, Venice (2003) 237
19. M. Maltoni et al, Phys. Rev. **D68**, 113010 (2003); Phys. Rev. **D67**, 013011 (2003)
20. G. Fogli et al, Phys. Rev. **D66**, 053010 (2002)
21. A. B. Balantekin and H. Yuksel, Phys. Rev. **D68**, 113002 (2003)
22. G. Fiorentini et al, Phys. Lett. **B558**, 15 (2003); H. Nunokawa, W. C. Teves and R. Zukanovich, JHEP **11**, 020 (2003)
23. M. Gonzalez-Garcia et al, Phys. Rev. **D63**, 033005 (2001)
24. G. Barr, T. K. Gaisser and T. Stanev, Phys. Rev. **D39**, 3532 (1989).
25. http://eps2003.physik.rwth-aachen.de.
26. Particle Data Group, K. Hagiwara et al, Phys. Rev. **D66**, 010001 (2002).
27. A. Zee, Phys. Lett. **B93**, 389 (1980).
28. K. S. Babu, Phys. Lett. **B203**, 132 (1988).
29. M. Hirsch and J. W. F. Valle, New J. Phys. **6**, 76 (2004) [hep-ph/0405015]
30. R. N. Mohapatra and J. W. F. Valle, Phys. Rev. **D34**, 1642 (1986).
31. J. Bernabeu et al, Phys. Lett. **B187**, 303 (1987); G. C. Branco, M. Rebelo and J. W. F. Valle, Phys. Lett. **B225**, 385 (1989); N. Rius and J. W. F. Valle, Phys. Lett. **B246**, 249 (1990); F. Deppisch and J. W. F. Valle, hep-ph/0406040.
32. J. Schechter and J. W. F. Valle, Phys. Rev. **D23**, 1666 (1981).
33. M. Doi et al, Phys. Lett. **B102**, 323 (1981); S. Bilenky et al, Phys. Lett. B **94** 49 (1980)
34. K. Dick, M. Freund, M. Lindner and A. Romanino, Nucl. Phys. **B562**, 29 (1999)
35. M. Apollonio et al, Phys. Lett. **B466**, 415 (1999); F. Boehm et al, Phys. Rev. **D64**, 112001 (2001)
36. J. Schechter and J. W. F. Valle, Phys. Rev. **D21**, 309 (1980).
37. M. Freund, Phys. Rev. **D64**, 053003 (2001)
38. E. K. Akhmedov et al, hep-ph/0402175.
39. C. Yanagisawa, Proc. of AHEP2003, published at JHEP, PRHEP-AHEP2003/062, accessible from http://ific.uv.es/ahep/.
40. E. K. Akhmedov et al, JHEP **0405** 057 (2004); M. Blennow et al, Phys. Rev. **D69**, 073006 (2004)
41. J. Schechter and J. W. F. Valle, Phys. Rev. **D25**, 2951 (1982)
42. D. O. Caldwell and R. N. Mohapatra, Phys. Rev. **D48**, 3259 (1993).
43. A. Ioannisian and J. W. F. Valle, Phys. Lett. B **332** 93 (1994)
44. H. V. Klapdor et al, hep-ph/9910205.
45. H. Klapdor etal, Phys. Lett. B **586** (2004) 198
46. A. Osipowicz, et al, hep-ex/0109033.
47. S. Pastor, these volume; S. Hannestad, hep-ph/0404239; G. Fogli etal, hep-ph/0408045
48. A. Aguilar et al, Phys. Rev. **D64**, 112007 (2001)
49. J. T. Peltoniemi and J. W. F. Valle, Nucl. Phys. **B406**, 409 (1993)
50. J. T. Peltoniemi, D. Tommasini and J. W. F. Valle, Phys. Lett. **B298**, 383 (1993).
51. M. Maltoni et al, Nucl. Phys. **B643**, 321 (2002), [hep-ph/0207157].
52. M. Maltoni, T. Schwetz and J. W. F. Valle, Phys. Rev. **D65**, 093004 (2002)
53. E. D. Church, K. Eitel, G. B. Mills and M. Steidl, Phys. Rev. **D66**, 013001 (2002)
54. M. Maltoni and T. Schwetz, Phys. Rev. **D68**, 033020 (2003)
55. S. Pakvasa and J. W. F. Valle, Proc. of the Indian Nat. Acad. of Sciences, Vol. 70A, No.1, p.189 - 222 (2004), [hep-ph/0301061]
56. J. W. F. Valle, Prog. Part. Nucl. Phys. **26**, 91 (1991); for a good example see Ref. [28]
57. L. J. Hall, V. A. Kostelecky and S. Raby, Nucl. Phys. **B267**, 415 (1986).
58. N. Fornengo et al, Phys. Rev. **D65**, 013010 (2002)
59. P. Huber and J. W. F. Valle, Phys. Lett. **B523**, 151 (2001), [hep-ph/0108193].
60. O. G. Miranda, M. A. Tortola and J. W. F. Valle, hep-ph/0406280.
61. P. Huber, T. Schwetz and J. W. F. Valle, Phys. Rev. **D66**, 013006 (2002); Phys. Rev. Lett. **88**, 101804 (2002)